Ibn Al-Haitham Journal for Pure and Applied Sciences
Journal homepage: jih.uobaghdad.edu.iq
PISSN: 1609-4042, EISSN: 2521-3407
IHJPAS. 2026; 39(1)

Effects of a Chelated Multi-Micronutrient Nanofertilizer on the Liver of Albino Rats: A Biochemical and Histopathological Assessment

Amenah AbdulJabbar Ibrahim [1*] and **Mohammed Mahdi Jawad** [2]
[1,2] Department of Biology, College of Education for Pure Science (Ibn Al-Haitham), University of Baghdad, Baghdad, Iraq
*Corresponding Author

Received: 11/June/2025
Accepted:30/September/2025
Published: 20/January/2026
doi.org/10.30526/39.1.4226

Abstract

Nanofertilizers offer a promising solution to increase crop yields amid increasing population pressure. Yet there have been safety concerns about their use, particularly in challenging conditions. This work was designed to assess the toxicological effects of a chelated multi-micronutrient nanofertilizer on albino rats (*Rattus norvegicus*) as non-target organisms, focusing on the liver, which has important metabolic functions. Thirty-five animals were weighed and randomly divided into 5 groups (n=7). A negative control group was included, and four experimental groups (C1-C4) were given the test item. The dosing regimen for the experimental groups was 15 oral doses of nanofertilizer every other day for 29 days. All the groups were treated with different doses (62.5, 125, 250, and 500 mg/kg, respectively). Biochemical analyses revealed a statistically significant reduction in lactate dehydrogenase (LDH) levels in groups C2 through C4 (661.00 ± 181.67, 572.43 ± 187.62, and 577.86 ± 110.84 U/L, respectively) compared to both the control (919.86 ± 232.08 U/L) and C1 (880.00 ± 119.17 U/L) groups. In contrast, serum total protein concentrations exhibited a marked increase across all treatment groups (C1–C4: 74.36 ± 3.91, 68.49 ± 5.88, 70.47 ± 7.93, and 68.14 ± 3.84 g/L, respectively), relative to the control (59.29 ± 5.49 g/L). This rise in total protein was mainly due to a significant increase in serum globulin, whereas albumin showed a marked decrease. Histological examination showed dose-dependent hepatotoxicity in all treatment groups. These results indicated that a sub-lethal dose of this nanofertilizer has the potential to elicit observable hepatotoxicity, underscoring the need for careful application and further toxicological evaluations.

Keywords: Nanofertilizers; Liver toxicity; Albino rats; Lactate Dehydrogenases (LDH); Total protein; Histopathology.

1. Introduction

Nanofertilizers are a new generation of agrochemicals, synthesized at the nanoscale, that improve the efficiency of nutrient delivery and uptake by plants. Their distinct physicochemical traits represent exciting opportunities to improve agricultural yields and reduce the environmental burden associated with conventional fertilizer application[1]. These nanomaterials are generally produced by physical (top-down), chemical (bottom-up), or biological-facilitated approaches[2,3]. These are mostly grouped in three main categories (macronutrient-based, micronutrient-based, and bio-derived nanoscale formulations. Some nanofertilizers are developed to supply a single nutrient, and others to supply multiple elements[2]. Human exposure to nanofertilizer-derived nanoparticles is likely to occur through various pathways; ingestion is the most prominent. The plants grown with nanofertilizer treatments may uptake and accumulate nanoparticles within the edible plant parts of the human food chain [4,5]. Furthermore, in stressful agro-ecological situations, such as drought with high temperatures and humidity, the

nanoparticles can persist in soils or may be inadvertently taken up by plants or even aerosolized as PM2.5. Inhalation of nanoparticle-loaded dust further poses additional health hazards, such as oxidative stress, DNA damage, and systemic toxicity[1,6,7]. Emerging evidence has revealed that these major organs (liver, kidney, heart, and spleen) could be affected by both short-term exposure and long-term administration of nanoparticles[1].

The liver is obviously involved, as nanoparticles may come into contact with it due to the use of nanofertilizers in crops, since it plays a key role in the removal of various xenobiotics, including NPs, which can remain in this organ at up to 99%[8].

To better understand how the liver performs its essential roles, its microarchitecture can be described by the acinus model, where hepatic tissue is organized into irregular units (acini) centred around portal tracts, especially the portal vein. Blood flows from these tracts to central veins, generating oxygen and nutrient gradients that define three metabolic zones[9]. Portal tracts are bordered by hepatocytes, forming the limiting plate, where three lobules meet. Portal venules appear thin-walled, while hepatic arterioles have a single layer of elongated smooth muscle cells, lightly stained in hematoxylin and eosin (H&E) sections. Small bile ducts are lined with cuboidal epithelium, and larger ducts contain smooth muscle, though in rats, intrahepatic bile ducts lack muscle and are supported by connective tissue. Bile canaliculi, found between hepatocytes, are too fine to be visualized with standard H&E staining[9].

At the cellular level, hepatocytes, comprising approximately 80% of the liver's mass, are large polyhedral cells characterized by pale nuclei of variable size, some exhibiting polyploidy, and cytoplasm with a granular appearance containing vacuoles resulting from glycogen and lipid extraction. These cells are organized into double-layered plates, separated by bile canaliculi with microvilli, and sealed by tight junction complexes; their external surfaces are adjacent to fenestrated hepatic sinusoids, facilitating selective exchange with the space of Disse. The hepatic parenchyma also includes various specialized cell types such as fenestrated endothelial cells, Kupffer macrophages, stellate cells rich in vitamin A, and biliary epithelial cells, as well as fibroblasts, smooth muscle cells, neuroendocrine cells, hematopoietic cells, stem cells, and pit cells, a distinct population of natural killer cells[10,11].

Within this physiological context, the liver is distinct in that it receives blood from two vascular beds: oxygenated blood via the hepatic artery (a branch of the celiac trunk) and nutrient-rich venous drainage from the gut via the portal vein. This venous drainage is supplied by the superior and inferior mesenteric, gastroepiploic, splenic, and pancreatic veins[10]. Venous blood from the liver drains on a more straightforward path via the hepatic veins into the inferior vena cava. Ductal sensitivities to the toxic insult are associated with variation in the branching patterns of hepatic vessels[10]. Because of its rich vascularity and central role in detoxification, as evidenced by liver function disorders even at relatively low exposure levels. They engage with hepatocytes to induce inflammation and oxidative stress [12]. Kupffer cells mediate this response by phagocytosing NPs and secreting pro-inflammatory mediators. Nanoparticles also inhibit liver enzymes, affecting detoxification. The degree of liver injury depends on the size, composition, and administration route of NPs[12,13].

Recent reports on the effects of nanoparticles in the liver underscore the importance of robust hepatic biomarkers[14]. LDH, which plays a central role in the lactate-to-pyruvate conversion through NAD^+/NADH turnover, is an integral part of cellular energy metabolism. In addition, LDH is a non-specific biomarker used in the clinic to evaluate tissue damage and disease progression [14]. Furthermore, it is no less important to monitor changes in serum proteins (albumin, globulin, and total protein) than enzymes, since these are major biochemical indicators of liver synthetic function. They are also crucial for nutrient transport, oncolysis, and immune enhancement. Early liver injury ensues when they are disrupted by nanoparticles[12]. Therefore, it was planned to investigate the downsides of nanofertilizers on non-target organisms, even though their benefits for agricultural production are weighed against the possibility of environmental accumulation and entry into the food chain.

2. Materials and Methods

2.1. Laboratory Animals

Thirty-five male albino rats (Rattus norvegicus) of 7-10 weeks old, weighing between 176 and 350 g, were used in this experiment. Animals were obtained from two authenticated sources: the Iraqi Center for Genetics and Cancer Research at Al-Mustansiriyah University and the National Center for Drug Control and Research, affiliated with the Ministry of Health. Rats were kept in standard animal care conditions, caged with sawdust bedding, and maintained under standard laboratory conditions; they had access to a balanced chow and tap water ad libitum throughout the study. Two weeks of acclimatization were provided to the rats before the experimental procedures to stabilize physiological parameters and facilitate adaptation to environmental conditions. The animals were weighed and individually identified, after which they were divided into one control group and four treatment groups, with seven rats per group: C1 (62.5 mg/kg), C2 (125 mg/kg), C3 (250 mg/kg) , and C4 (500 mg/kg). Both experimental groups consisted of rats aged 7-10 weeks.

2.2. Nanofertilizer and Oral Administration

A glycine-chelated multi-micronutrient nanofertilizer including iron (Fe), zinc (Zn), copper (Cu), manganese (Mn), boron (B), and molybdenum (Mo) was procured from a certified agricultural supplier based in Baghdad. The manufacturer's recommended concentration for foliar application (1 g/L) was used as a reference , assuming 1 L of water weighs about 1 kg. The experimental doses of 62.5, 125, 250, and 500 mg/kg were determined from this reference. The ultimate dose for each animal was determined based on the mean body weight of all animals from both groups (15). Verification of the chosen doses was performed in a pilot trial before this procedure, and subsequent treatments were administered to groups C1 through C4. Each rat was given a single oral dose by gavage at 24-h intervals using a 16-gauge, ball-tipped stainless steel feeding needle, 38 mm in length. Animals were weighed again after the last dose to monitor weight loss. Then they were anesthetized with chloroform and dissected 24 h after the last injection. Study of biochemical parameters. Blood samples taken at cardiac puncture were used to measure biochemistry; livers were isolated, weighed, then fixed in 10% formalin for 24 hours, followed by preservation in 70% ethyl alcohol before histological examination.

2.3. Biochemical Analysis

Blood samples were drawn into 1 ml heparin-lithium solution precoated Eppendorf tubes for anticoagulation. Each tube was then gently mixed 8-10 times according to the manufacturer's instructions to ensure proper mixing of blood and anticoagulant. Subsequently, serum biochemical parameters, including LDH, TP, albumin (A), globulin (G), as well as the albumin to globulin (A/G) ratio, were quantified using a veterinary dry chemistry analyzer (Seamaty, China), with its specific kit (Seamaty, REF: AW01980, LOT: 9231720). Results were produced by analysis and printed after about 12 minutes from loading the sample.

2.4. Histopathological Study

Histological preparation was performed in accordance with the protocol[16]. Liver tissues underwent stepwise dehydration through a graded ethanol series, followed by clearing in xylene and embedding in paraffin wax. Tissue blocks were sectioned at a thickness of 4 μm using a rotary microtome. The sections were stained with hematoxylin and eosin (H&E) as well as Masson's trichrome stains[16,17]. Stained slides were evaluated under a light microscope, and representative fields were digitally imaged to assess and record the histoarchitectural features.

2.5. Statistical Analysis

Data analysis was performed using IBM SPSS Statistics software (Version 23). One-way analysis of variance (ANOVA) was applied to evaluate the presence of statistically significant differences among the experimental groups. Where significant differences were detected, the least significant difference (LSD) post hoc test was employed to identify specific pairwise group differences. All results are expressed as mean values and standard deviations (mean ± SD). A significance threshold of $p \leq 0.05$ was adopted for all statistical tests[18].

3. Results

3.1. Biochemical Analysis

3.1.1 LDH Levels

The results in **Figure 1** showed a statistically significant decrease in LDH enzyme levels (P = 0.001) began from the C2 experimental group to the C4 group according to the control and the C1 group.

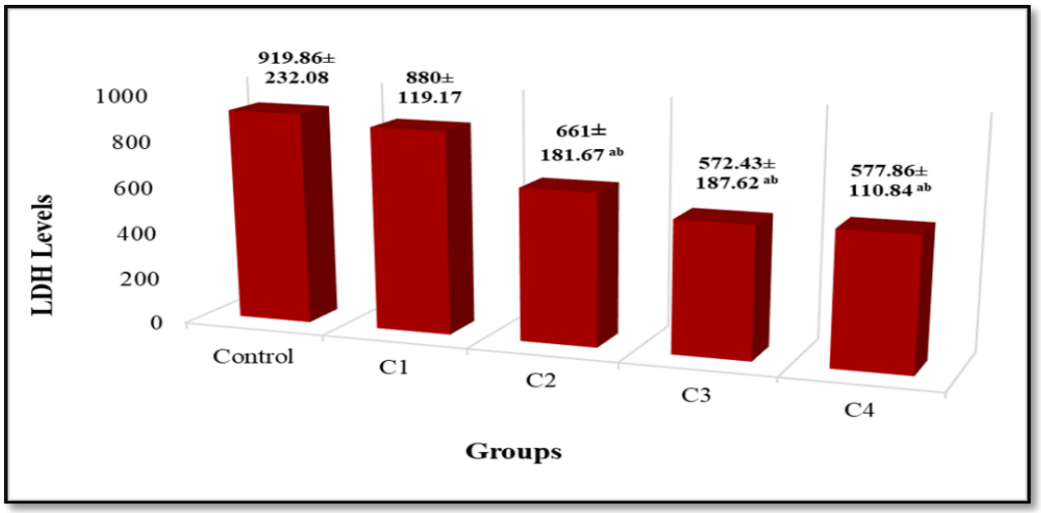

Figure 1. LDH enzyme levels (U/L) presented as mean ± S.D. Significant differences ($P \leq 0.05$) indicated by letters: (a) significantly different from control; (b) significantly different from group C1; LSD = 188.16.

3.1.2 Serum proteins Concentration

As presented in **Table 1**, all experimental groups (C1-C4) exhibited a statistically significant increase in total serum protein and globulin concentrations, accompanied by a marked decrease in albumin levels ($p < 0.001$) when compared to the control group. The most notable result was the increase in globulin, which, in turn, contributed significantly to the decrease in the albumin-to-globulin ratio, despite the substantial decrease in albumin. (A/G) ratio.

Table 1. Total protein, albumin, globulin concentrations and A/G ratio

Groups	Parameters			
	Total protein (Mean±S.D.)	Albumin (Mean±S.D.))	Globulin (Mean±S.D.)	Albumin/Globulin (Mean±S.D.)
Control	59.29±5.49	39.64±1.92	22.07±8.30	2.20±0.34
C1	74.36±3.91 a	35.00±3.01 a	39.34±3.08 a	0.89±0.11 a
C2	68.49±5.88 a	32.37±2.92 a	36.10±4.26 a	0.91±0.12 a
C3	70.47±7.93 a	34.83±4.60 a	35.64±5.19 a	0.99±0.17 a
C4	68.14±3.84 ab	31.39±3.86 a	36.73±5.31 a	0.89±0.26 a
P-Value	<0.001**	<0.001**	<0.001**	<0.001**
LSD	6.13	3.7	6.01	0.24

* The small letters indicate a significant difference: (a) vs. control, (b) vs. C1, $p \leq 0.05$

3.2. Histopathological changes in the liver

Histopathological examination of the control rats' livers, stained with H&E, showed that a normal hepatic lobular structure was maintained. Hepatocytes were well-maintained with homogeneous cytoplasm and a centrally located nucleus without any histopathological changes, as shown in **Figure 2** In contrast, as shown in **Figure 3**, the liver tissue of the C1 group showed structural disarray of hepatic cords with portal vein congestion and sinusoidal dilation. These changes were associated with ductular hyperplasia, lymphocytic infiltrate and foci of necrosis and inflammation. In contrast, the lesions in group C2 (**Figure 4**) are more prominent: trabecular rupture, marked dilation and congestion of both central veins and portal veins, dilated portal venules and extended ductular reaction. Additional findings comprised lymphocytic

aggregates, focal necrosis, sinusoidal widening, and both macrovesicular and microvesicular steatosis, as well as scattered inflammatory infiltrates. By contrast, **Figure 5** (group C3) showed a persistent architectural derangement, including lymphocytic infiltration, portal congestion, hepatocyte necrosis, sinusoidal dilation, macrovesicular and microvesicular lipid accumulation, and nuclei with pyknosis. **Figure 6** (group C4) showed the advanced changes of severe distortion in trabecular architecture, oedema, degenerative lesions in portal and central veins, widening of sinusoidal spaces with lymphocytic and inflammatory cells infiltration and focal area hepatocellular necrosis. Masson's trichrome stain was used for additional evaluation of fibrotic changes and collagen distribution in liver specimens. **Figure 7** Control rats showed normal hepatic architecture with no evidence of collagen deposition or fibrosis. Group C1 (**Figure 8**) showed early fibrotic changes, including trabecular disarray, mild portal and pericentral fibrosis, a lymphocytic infiltrate, and widening of the central vein. Furthermore, **Figure 9** (group C2) showed a more marked fibrosis pattern, including trabecular collapse, periportal collagen deposition, bridging from the portal to the central area, and dense inflammatory infiltrates. The fibrotic thickening in the portal zones and portal-portal bridging, mild pericentral collagen deposits, and persistent lymphocytic infiltration were observed in group C3 later (**Figure 10**). Finally, group C4 (**Figure 11**) revealed the most severe changes, including extensive periportal fibrosis, fibrotic connections between portal tracts, disorganized trabeculae, and sustained inflammatory cell infiltration.

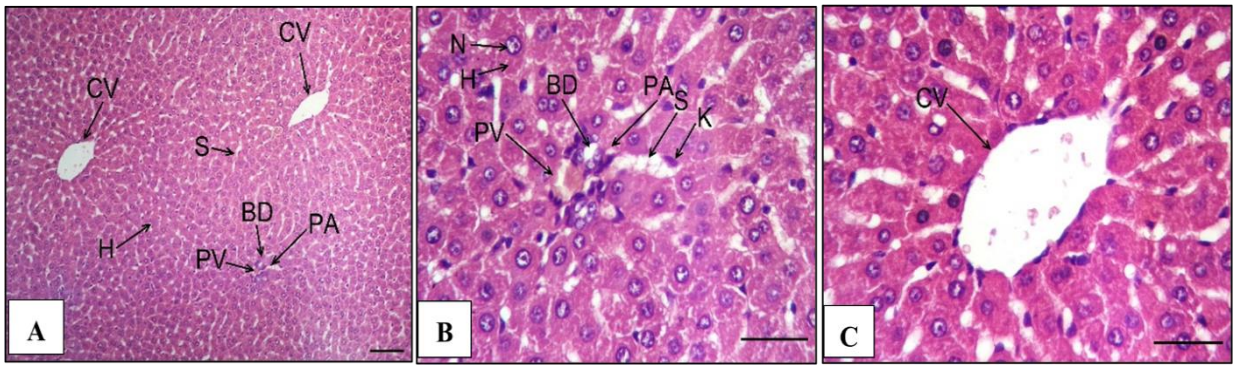

Figure 2. A transverse section (T.S.) of the liver from a control rat (*Rattus norvegicus*) shows normal hepatocytes, (H) with normal nuclei (N), normal hepatic trabecular architecture, central vein (C.V.), portal area (PA) containing portal vein (PV) and bile duct (BD), sinusoids (S), and Kupffer cells (K). Stained with H&E. A: 10× magnification; B and C: 40× magnification. Scale bar = 100 µm.

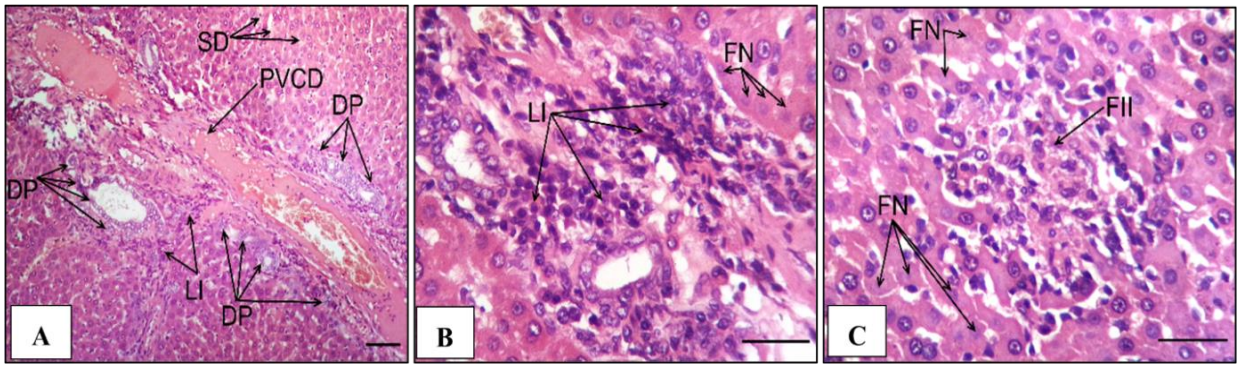

Figure 3. A transverse section (T.S.) of the liver from a C1 group rat (*Rattus norvegicus*) shows disruption of the hepatic trabecular architecture, portal vein congestion and dilation (PVCD), Sinusoidal dilation (SD), ductular proliferation (DP), lymphocytic infiltration, focal necrosis (FN), and focal inflammatory infiltration (FII). Stained with H&E. A: 10× magnification; B and C: 40× magnification. Scale bar = 100 µm.

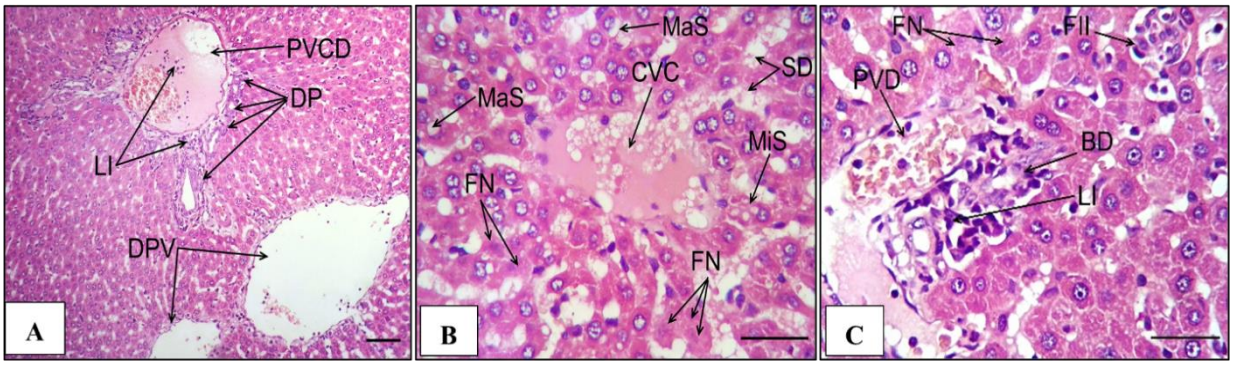

Figure 4. A transverse section (T.S.) of the liver from a C2 group rat (*Rattus norvegicus*) shows disruption of the hepatic trabecular architecture, portal vein congestion and dilation (PVCD), dilated portal venules (DPV), ductular proliferation (DP), lymphocytic infiltration (LI), focal necrosis (FN), central vein congestion (CVC), Sinusoidal dilation (SD), macrovascular steatosis (MaS), microvascular steatosis (MiS), portal vein dilation (PVD), and focal inflammatory infiltration (FII). Stained with H&E. A: 10× magnification; B and C: 40× magnification. Scale bar = 100 µm.

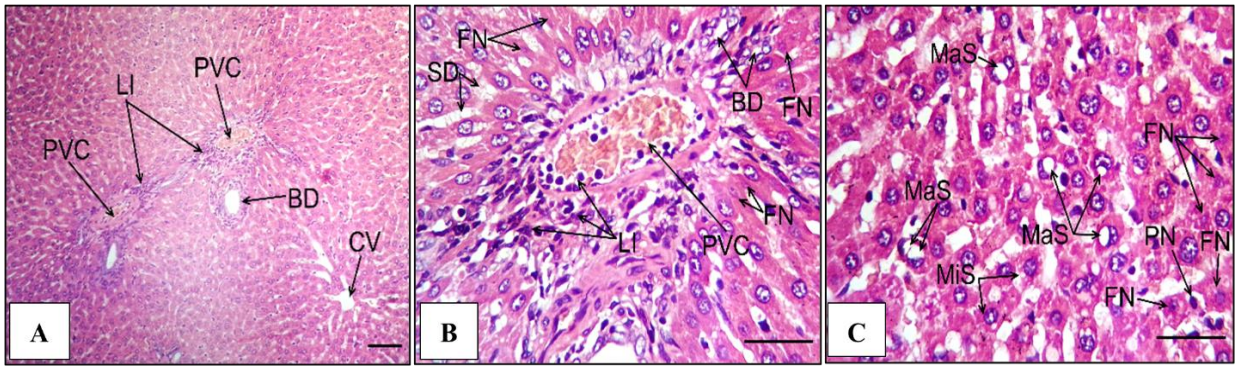

Figure 5. A transverse section (T.S.) of the liver from a C3 group rat (*Rattus norvegicus*) shows disruption of the hepatic trabecular architecture, lymphocytic infiltration (LI), portal vein congestion (PVC), focal necrosis (FN), Sinusoidal dilation (SD), macrovascular steatosis (MaS), microvascular steatosis (MiS), and pycnotic nucleus (PN). Stained with H&E. A: 10× magnification; B and C: 40× magnification. Scale bar = 100 µm.

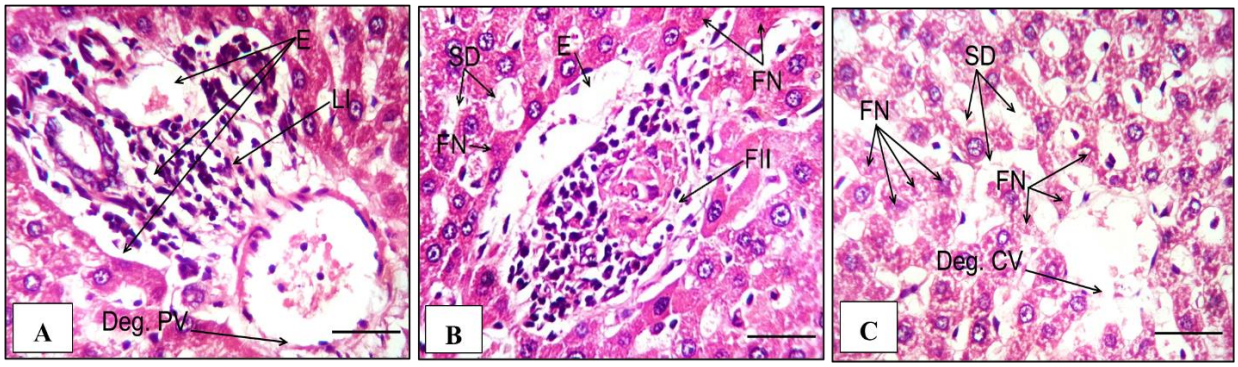

Figure 6. A transverse section (T.S.) of the liver from a C4 group rat (*Rattus norvegicus*) shows disruption of the hepatic trabecular architecture, lymphocytic infiltration (LI), Oedema (E), focal necrosis (FN), degenerative portal vein (Deg. PV), focal inflammatory infiltration (FII), sinusoidal dilation (SD), and degenerative central vein (Deg. CV). Stained with H&E. 40× magnification. Scale bar = 100 µm.

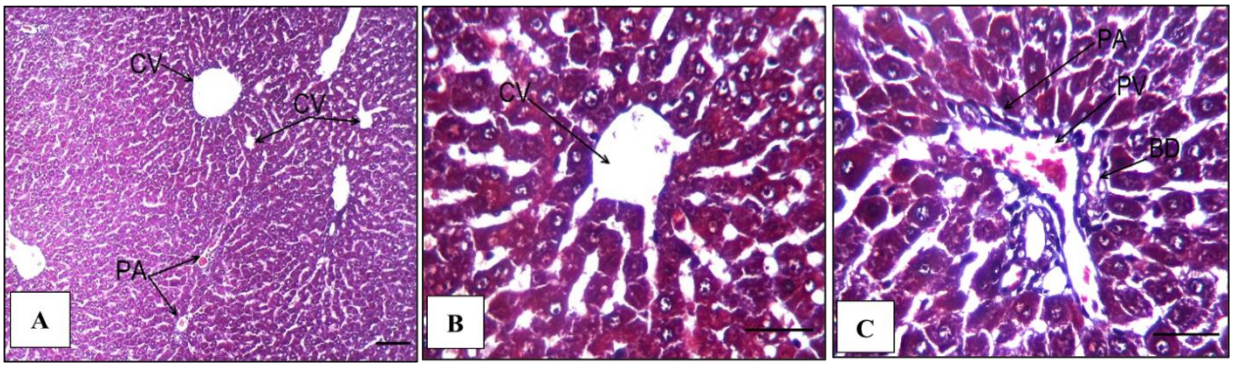

Figure 7. A transverse section (T.S.) of the liver from a control group of rats (*Rattus norvegicus*) shows normal hepatic trabecular architecture, central vein (CV), portal area (PA) with portal vein (PV) and bile duct (BD). Stained with Masson's trichrome stain. A: 10x magnification; B and C: 40x magnification. Scale bar = 100 µm.

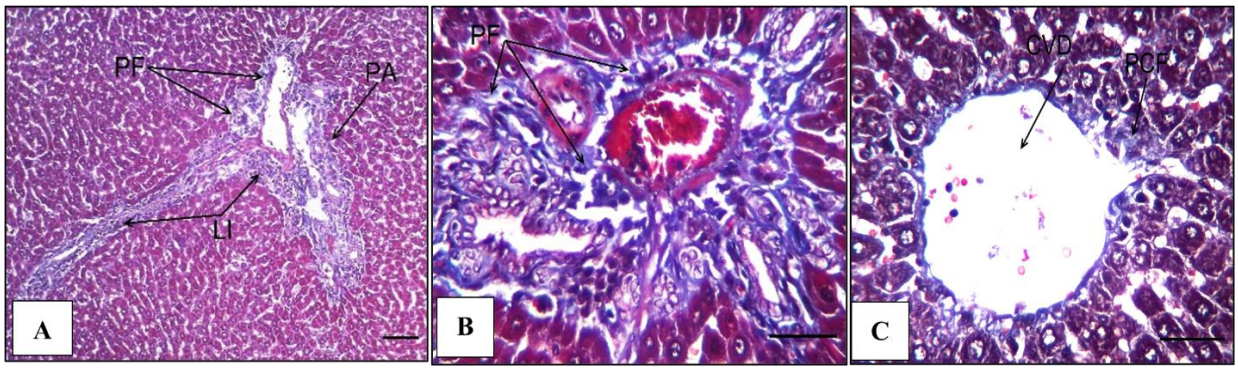

Figure 8. A transverse section (T.S.) of the liver from a C1 group rat (*Rattus norvegicus*) shows disruption of the hepatic trabecular architecture, mild portal fibrosis (PF), lymphocytic infiltration (LI), central vein dilation (CVD), and mild pericentral fibrosis (PCF). Stained with Masson's trichrome stain. A: 10x magnification; B and C: 40x magnification. Scale bar= 100 µm.

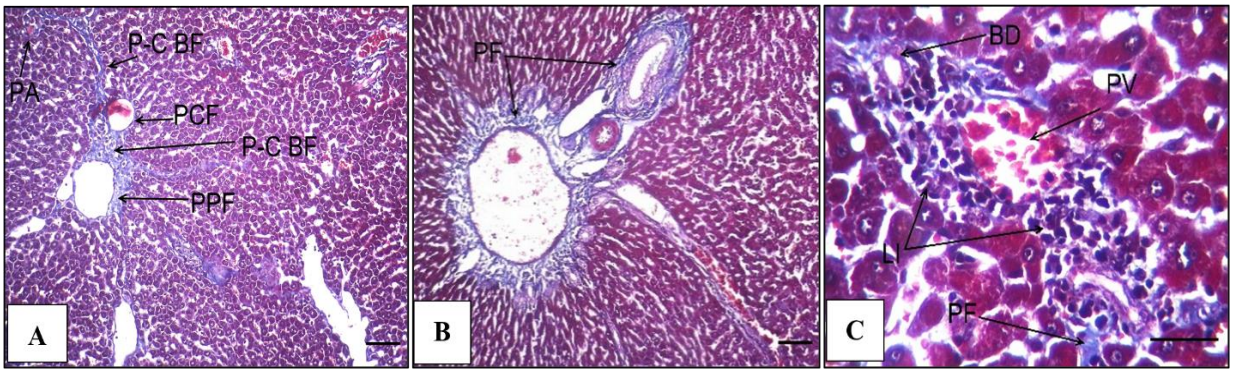

Figure 9. A transverse section (T.S.) of the liver from a C2 group rat (*Rattus norvegicus*) shows disruption of the hepatic trabecular architecture, periportal fibrosis (PPF), portal-central bridging fibrosis (P-C BF), pericentral fibrosis (PCF), periportal fibrosis (PPF), portal fibrosis (PF), and lymphocytic infiltration (LI). Stained with Masson's trichrome stain. A and B: 10x magnification; C: 40x magnification. Scale bar = 100 µm.

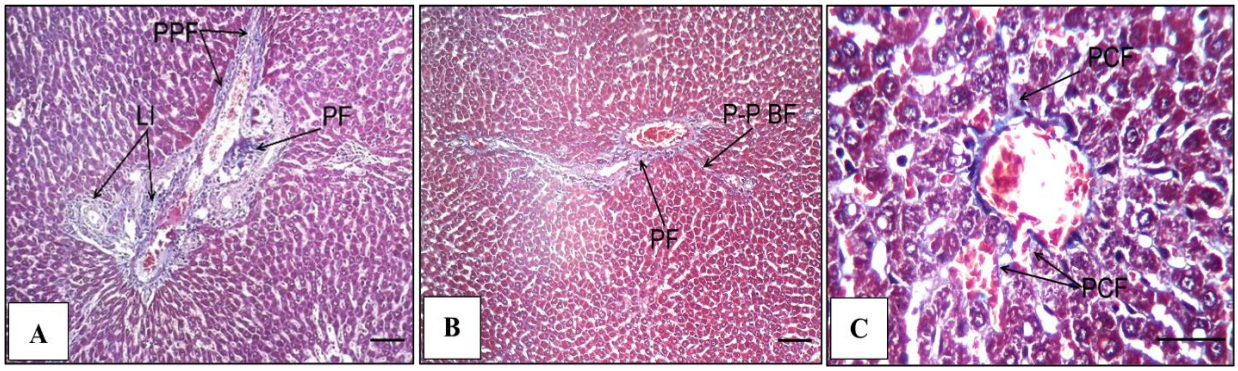

Figure 10. A transverse section (T.S.) of the liver from a C3 group rat (*Rattus norvegicus*) shows disruption of the hepatic trabecular architecture, periportal fibrosis (PPF), lymphocytic infiltration (LI), portal fibrosis (PF), portal-portal bridging fibrosis (P-P BF) and mild pericentral fibrosis (PCF). Stained with Masson's trichrome stain. A and B: 10x magnification; C: 40x magnification. Scale bar = 100 µm.

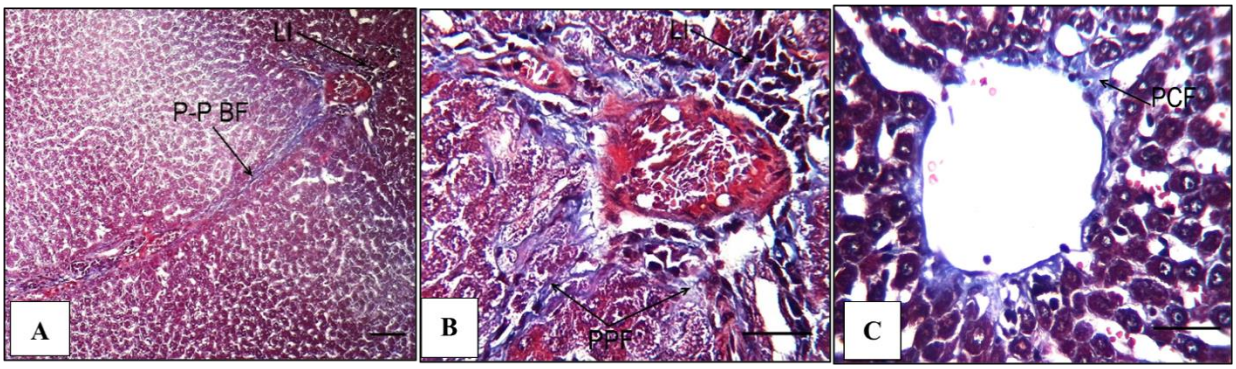

Figure 11. A transverse section (T.S.) of the liver from a C4 group rat (*Rattus norvegicus*) shows disruption of the hepatic trabecular architecture, lymphocytic infiltration (LI), portal-portal bridging fibrosis (P-P BF), periportal fibrosis (PPF), and mild pericentral fibrosis (PCF). Stained with Masson's trichrome stain. A: 10x magnification; B and C: 40x magnification. Scale bar = 100 µm.

4. Discussion

A significant reduction in lactate dehydrogenase (LDH) activity was observed following exposure to the nanofertilizer, consistent with previous studies that reported similar outcomes after nanoparticle exposure[19]. This reduction is attributed to the displacement of essential metal ions from the enzyme's active site and the formation of inhibitory complexes that disrupt enzyme function[19,20]. LDH assay is a well-established technique for analyzing NP-induced cytotoxicity, showing a dose-dependent effect: LDH levels increase at low NP concentrations due to membrane damage or lysis, and decrease at higher concentrations due to enzyme inactivation or adsorption to NP surfaces [21]. On the other hand, high levels of LDH have also been observed in PC12 cells exposed to manganese trioxide (Mn_3O_4) nanoparticles, suggesting substantial cellular damage and membrane disruption[22]. The current research also revealed a marked increase in total protein (TP), mainly due to a significant rise in globulin, accompanied by a reduction in albumin concentration. On the contrary, a marked decline in total protein content has been reported in rats treated with copper nanoparticles at all tested doses (50, 100, and 200 mg/kg), indicating hepatocellular damage and impairment of liver protein production[24]. In contrast, higher total protein and albumin levels were recorded in rats treated with molybdenum trioxide nanoparticles (MoO_3-NPs) or that consumed beans fertilised with these particles[20]. Concurrently, studies also showed that application of iron oxide nanoparticles (Fe_3O_4 NPs) and phytochemicals separately maintained liver protein synthesis at a normal level; however, their combined exposure regulated protein levels, suggesting multicomplex interactions that influence liver function and protein synthesis [24]. In addition, the reduction in albumin observed in the present study is equivalent to hypoalbuminemia and may be secondary to

decreased synthesis and systemic inflammation. In inflammatory conditions, increased vascular permeability allows albumin to enter the interstitial spaces, reducing circulating levels. Therefore, this system may be responsible for the changes in the protein profile observed in our results[25]. Histological examination of liver tissue revealed progressive injury, including trabecular disruption, sinusoidal congestion, ductular proliferation, inflammatory infiltration, necrosis, steatosis, and fibrosis. These alterations are consistent with established nanoparticle-induced hepatotoxic effects described in the literature. For example, disorganized lobular structure, Kupffer cell proliferation, inflammatory cell infiltration, and amyloid-like deposits have been reported following exposure to ZnO nanoparticles[26,27]. Pyknosis, microvesicular steatosis, vacuolation, extensive necrosis and fibrosis in liver tissues were also found when exposed to large amounts of CuO NPs[28]. These histological alterations could be ascribed to the production of reactive oxygen species (ROS) that mediate inflammation, inhibit tissue remodeling, and induce cell death[29]. In addition, MoO_3 NPs exposure induced inflammatory infiltration and the changes in sinusoids in the liver, implying a dose-dependent process of hepatic injury[19,30]. The liver, one of the main organs involved in nanoparticle retention, is vulnerable to oxidative and inflammatory injury[12,13]. Additionally, the size of particles interplays with Kupffer cells and will determine the hepatic responses modulated between necrosis/congestion or granuloma formation[8,31]. The relationship between liver disease and the albumin/globulin (A/G) ratio is also relevant; this ratio is typically greater than one, but fibrosis or chronic inflammation leads to decreased liver function, reduced albumin production, and increased globulin levels due to immune system overactivation, resulting in a reversal of this ratio[32]. Overall, the findings of the current study are consistent with existing evidence, confirming that nanofertilizer exposure, particularly at higher doses, induces complex and multifactorial liver injury.

5. Conclusion

Agricultural nanofertilizers that are used for plant nutrition and growth requirements are harmful to non-targeted organisms, including mammals that are used as a model in experiments.

Acknowledgment

The authors would like to thank the Department of Biology, College of Education for Pure Sciences (Ibn Al-Haitham), University of Baghdad, for their support and assistance during this research.

Conflict of Interest

The authors declare that they have no conflicts of interest.

Funding

There was no funding.

Ethical Clearance

The study was carried out in full adherence to established ethical standards for scientific research and in strict compliance with the institutional regulations governing the care and use of laboratory animals, following formal approval by the Institutional Ethics Committee (Approval No. EC-54, dated 24/12/2024).

References

1. Demeke ED, Benti NE, Terefe MG, Anbessa TT, Mengistu WM, Mekonnen YS. A comprehensive review on nano-fertilizers: preparation, development, utilization, and prospects for sustainable agriculture in Ethiopia. Nanoscale Adv. 2025;7(8):2131–2144. https://doi.org/10.1039/D4NA01068J.

2. Jaafar MF, Abdullah AK. Impact of interaction between nano particles and bacterial and amino fertilizers on growth and yield of wheat plant. Plant Arch. 2020;20(1):2829–35.
3. Imran HJ, Hubeatir KA, Aadim KA, Abd DS. Preparation methods and classification study of nanomaterial: a review. J Phys Conf Ser. 2021;1818(1):012127. https://doi.org/10.1088/1742-6596/1818/1/012127.
4. Wahab A, Batool F, Muhammad M, Zaman W, Mikhlef RM, Naeem M. Current knowledge, research progress, and future prospects of phyto-synthesized nanoparticles interactions with food crops under induced drought stress. Sustainability. 2023;15(20):14792. https://doi.org/10.3390/su152014792.
5. Mohammed MM. Disadvantages of using nano-particles as fertilizers in Iraq. IOP Conf Ser Earth Environ Sci. 2021;735(1):012043. https://doi.org/10.1088/1755-1315/735/1/012043.
6. Deschamps F. O-124 Atmospheric dust containing nanomaterials. Occupational Medicine. 2024;74(Supplement_1):0-. https://doi.org/10.1093/occmed/kqae023.0758.
7. Jawad MM, Ibrahim IAJ, Mahdi SS. Study the effect of some chemicals used locally in agricultural processes in Iraq on the DNA of some non-targeted organisms. J Mater Environ Sci. 2016;7(5):1576–80.
8. He Y, Wang Y, Wang L, Jiang W, Wilhelm S. Understanding nanoparticle-liver interactions in nanomedicine. Expert Opin Drug Deliv. 2024;21(6):829–43. https://doi.org/10.1080/17425247.2024.2375400.
9. Maynard RL, Downes N. Anatomy and histology of the laboratory rat in toxicology and biomedical research. 1st ed. Cambridge (MA): Academic Press; 2019. 378 p. https://doi.org/10.1016/B978-0-12-811837-5.00001-0.
10. Foster JR. Liver. In: Leininger JR, Bradley AE, editors. Boorman's pathology of the rat. 2nd ed. Amsterdam: Elsevier; 2018. p. 81–105.
11. Bilzer M, Roggel F, Gerbes AL. Role of Kupffer cells in host defense and liver disease. Liver Int. 2006;26(10):1175–86. https://doi.org/10.1111/j.1478-3231.2006.01342.x.
12. Ghareeb OA, Ali QA. Hepatotoxicity induced by some metal nanoparticles in vivo: review. J Clin Med Rev. 2024;3(1). https://doi.org/10.58489/2836-2330/017.
13. Cornu R, Béduneau A, Martin H. Influence of nanoparticles on liver tissue and hepatic functions: a review. Toxicology. 2020;430:152344. https://doi.org/10.1016/j.tox.2019.152344.
14. Klein R, Nagy O, Tóthová C, Chovanová F. Clinical and diagnostic significance of lactate dehydrogenase and its isoenzymes in animals. Vet Med Int. 2020;2020:5346483. https://doi.org/10.1155/2020/5346483.
15. Erhirhie EO, Ekene, NE, Ajaghaku DL. Guidelines on dosage calculation and stock solution preparation in experimental animals' studies. J Nat Sci Res. 2014;4(18):100–6.
16. Humason GL. Animal tissue techniques. San Francisco: W.H. Freeman; 1962. 468 p.
17. Kiernan JA. Histological and histochemical methods: theory and practice. 5th ed. Scion Publishing Ltd.; 2015. 592 p.
18. George D, Mallery P. IBM SPSS Statistics 23 step by step: a simple guide and reference. 14th ed. New York: Routledge; 2016;400p. http://doi.org/10.4324/9781315545899.
19. Asadi F, Mohseni M, Dadashi Noshahr K, Soleymani FH, Jalilvand A, Heidari A. Effect of molybdenum nanoparticles on blood cells, liver enzymes, and sexual hormones in male rats. Biol Trace Elem Res. 2017;175(1):50–6. https://doi.org/10.1007/s12011-016-0765-5.
20. Shaban EE, Salama DM, Abd El-Aziz ME, Ibrahim KS, Nasr SM, Desouky HM, Elbakry HFH. The effect of exposure to MoO_3-NP and common bean fertilized by MoO_3-NPs on biochemical, hematological, and histopathological parameters in rats. Sci Rep. 2022;12(1):12074. https://doi.org/10.1038/s41598-022-16022-8.
21. Han X, Gelein R, Corson N, Wade-Mercer P, Jiang J, Biswas P, Finkelstein JN, Elder A, Oberdörster G. Validation of an LDH assay for assessing nanoparticle toxicity. Toxicology. 2011;287(1–3):99–104. https://doi.org/10.1016/j.tox.2011.06.011.
22. Chen X, Wu G, Zhang Z, Ma X, Liu L. Neurotoxicity of Mn_3O_4 nanoparticles: apoptosis and dopaminergic neurons damage pathway. Ecotoxicol Environ Saf. 2020;188:109909. https://doi.org/10.1016/j.ecoenv.2019.109909.
23. Tang H, Xu M, Luo J, Zhao L, Ye G, Shi F, Lv C, Chen H, Wang Y, Li Y. Liver toxicity assessments in rats following sub-chronic oral exposure to copper nanoparticles. Environ Sci Eur. 2019;31(1):30. https://doi.org/10.1186/s12302-019-0214-0.

24. Kazaryan SA, Oganian SA, Vardanyan GS, Sidorenko AS, Hovhannisyan AA. Liver-targeting iron oxide nanoparticles and their complexes with plant extracts for biocompatibility. Beilstein J Nanotechnol. 2024;15:1593–602. https://doi.org/10.3762/bjnano.15.125.
25. Soeters PB, Wolfe RR, Shenkin A. Hypoalbuminemia: pathogenesis and clinical significance. J Parenter Enteral Nutr. 2019;43(2):181–93. https://doi.org/10.1002/jpen.1451.
26. Razooki SMM, Rabee AM. Evaluation of the toxicological effects of zinc oxide nanoparticles in albino male mice. Iraqi J Sci. 2020;61(1):42–58. https://doi.org/10.24996/ijs.2020.61.1.5.
27. Salman RA. Histopathological effect of zinc oxide nanoparticles on kidney and liver tissues in albino male mice. Ibn Al-Haitham J Pure Appl Sci. 2018;31(1):9–14. https://doi.org/10.30526/31.1.1844.
28. Ghonimi WAM, Alferah MAZ, Dahran N, El-Shetry ES. Hepatic and renal toxicity following the injection of copper oxide nanoparticles (CuO NPs) in mature male Westar rats: histochemical and caspase 3 immunohistochemical reactivities. Environ Sci Pollut Res. 2022;29(54):81923–37. https://doi.org/10.1007/s11356-022-21521-2.
29. Al-Musawi MMS, Al-Shmgani H, Al-Bairuty GA. Histopathological and biochemical comparative study of copper oxide nanoparticles and copper sulphate toxicity in male albino mice reproductive system. Int J Biomater. 2022;2022:4877637. https://doi.org/10.1155/2022/4877637.
30. Badi N, Fazelipour S, Naji T, Babaei M, Hessari AK. Histomorphometric and biochemical study of liver and thyroid hormones following administration of MoO_3 nanoparticles in female rats. Iran J Vet Med. 2022;16(2):188–201. https://doi.org/10.22059/IJVM.2021.330872.1005196.
31. Waris A, Sharif S, Naz S, Manzoor F, Jamil F, Hussain M, Choi YJ, Park YK. Hepatotoxicity induced by metallic nanoparticles at the cellular level: a review. Environ Eng Res. 2023;28(5):230147. https://doi.org/10.4491/eer.2022.625.
32. Li J, Li Z, Hao S, Wang J, Chen W, Dai S, Hou Z, Chen B, Zhang Y, Liu D. Inversed albumin-to-globulin ratio and underlying liver disease severity as a prognostic factor for survival in hepatocellular carcinoma patients undergoing transarterial chemoembolization. Diagnostic and Interventional Radiology. 2023;29(3):520-528. https://doi.org/10.5152/dir.2022.211166.